Journal of Bioresources and Bioproducts 10 (2025) 170–186

Contents lists available at ScienceDirect

Journal of Bioresources and Bioproducts

journal homepage: https://www.keaipublishing.com/en/journals/journal-of-bioresources-and-bioproducts/

Research Article

# Enhanced performance and reprocessability in polypropylene-lignin blends through plasma treatment

Emanuela Bellinetto[a], Sofia Regoli[a], Ruggero Barni[b], Carmen Canevali[c], Oussama Boumezgane[a], Luca Zoia[d], Claudia Riccardi[b], Stefano Turri[a], Gianmarco Griffini[a,*]

[a] Department of Chemistry, Materials and Chemical Engineering "Giulio Natta", Politecnico di Milano, Milano 20133, Italy
[b] Department of Physics "Giuseppe Occhialini", Università degli Studi di Milano-Bicocca, Milano 20126, Italy
[c] Department of Materials Science, Università degli Studi di Milano-Bicocca, Milano 20125, Italy
[d] Department of Earth and Environmental Science, Università degli Studi di Milano-Bicocca, Milano 20126, Italy

ARTICLE INFO

*Keywords:*
Lignin
Polypropylene
Plasma
Gliding arc tornado
Compatibilization

ABSTRACT

In this work, a new compatibilization strategy for polypropylene-lignin blends was presented, which did not rely on the use of solvents or other chemicals. Soda lignin was subjected to plasma treatment in an argon atmosphere employing a gliding-arc-tornado reactor configuration. The effect of this process was evaluated using electron paramagnetic resonance spectroscopy, nuclear magnetic resonance spectroscopy, differential scanning calorimetry, and thermogravimetric analysis, evidencing significant chemical-structural modifications in lignin, including an increased concentration of phenoxy radicals (60%) and depletion of hydroxyl functionalities (35%). Polypropylene-lignin blends incorporating 5% (*w/w*), 10% (*w/w*), and 20% (*w/w*) of either pristine or plasma-treated lignin were then prepared by melt-blending in a twin-screw extruder, and their thermo-mechanical and rheological properties were investigated in detail. As a result of the plasma-induced modifications occurred in lignin, blends incorporating the plasma-treated material exhibited greater thermo-oxidative stability, more favorable viscoelastic response, significantly improved mechanical performance (137% and 294% strain at break for polypropylene (PP) containing 5% (*w/w*) and 10% (*w/w*) of treated lignin, respectively), and enhanced thermo-mechanical reprocessability (> 95% retention of yield strength and strain at break after re-extrusion). This work provided the first demonstration of the effectiveness of plasma treatment as a viable and sustainable strategy to improve filler-matrix interactions in polypropylene-lignin blends without the use of solvents, chemical compatibilizers or additional wet-chemistry steps, paving the way for the development of lignin-based thermoplastic polyolefin materials with enhanced thermo-mechanical characteristics and improved reprocessability.

## 1. Introduction

Polypropylene (PP) is one of the most widely used polymeric materials on a global scale. Due to its low cost, high versatility and remarkable chemical and mechanical properties, it constitutes >20% in the volume of all commodity plastics consumed worldwide (Geyer et al., 2017). In 2021, the production of PP approached 76 million metric tons and is set to reach 100 million metric tons in 2029 (Wang et al., 2023). Considering that currently only 9% of the total plastic waste is effectively recycled, the large and

* Corresponding author.
*E-mail address:* gianmarco.griffini@polimi.it (G. Griffini).

https://doi.org/10.1016/j.jobab.2025.01.003

Available online 20 January 2025
2369-9698/© 2025 The Authors. Publishing Services by Elsevier B.V. on behalf of KeAi Communications Co. Ltd. This is an open access article under the CC BY-NC-ND license (http://creativecommons.org/licenses/by-nc-nd/4.0/)

increasing production volume of such materials and their proper waste management have become growing global concerns (Patrício Silva et al., 2020). In this context, reformulation of plastics with alternative materials from renewable sources may represent a valuable and parallel strategy to reduce the environmental burden associated with the end-of-life fate of common petrol-based polymers (Müller et al., 2019; Levchenko et al., 2022).

Lignin is the most abundant natural aromatic polymer on Earth, constituting 17%–33% of the mass of trees and plants (Kun and Pukánszky, 2017). It is biodegradable (Saito et al., 2012) and highly thermally stable (Li et al., 2013), it also has demonstrated the ability to act as a scavenger of oxidative radicals due to its aromatic structure (Stanzione and La Scala, 2016; Guilhen et al., 2017). Given this, using lignin in polymeric blends with PP to form biobased composites can be an excellent approach to reduce the carbon footprint of fossil-based polyolefin products while improving their thermo-oxidative stability, possibly preventing degradation phenomena during reprocessing (e.g., in the mechanical recycling phase) (Cicala et al., 2017; Kabir et al., 2019). Additionally, lignin is widely available as the waste product of the pulping industry, its inclusion in any value-added application may also be beneficial from a circular economy perspective (Bertella and Luterbacher, 2020; Bellinetto et al., 2024). In light of this, a variety of works investigated the effects of incorporating different lignin types into the PP matrix (Toriz et al., 2002; Dias et al., 2019; Ridho et al., 2022). While it is widely acknowledged that lignin can act as an exceptional natural anti-oxidant (Pouteau et al., 2003; Gregorová et al., 2005; Canetti et al., 2006), ultraviolet -blocking (Ye et al., 2016; Sadeghifar and Ragauskas, 2020; Anushikha and Gaikwad, 2023), and flame retardant additive (Lee et al., 2022; Zhao et al., 2023), its contribution to a simultaneous improvement or retention of the mechanical properties of PP remains unattainable without the use of a coupling agent (e.g., maleic anhydride-grafted polypropylene (MAn-g-PP), ethylene vinyl acetate) (Alexy et al., 2004; Atifi et al., 2017; Tanks et al., 2023). Indeed, given the high amount of hydroxyl functionalities present in the lignin structure and the absence of any polar group in PP, no synergistic interactions can be established between the two polymers, resulting in a heterogeneous composite material with poor mechanical properties (Duval and Lawoko, 2014; Kun and Pukánszky, 2017). As an example, it has been reported that the addition of 10% (*w/w*) lignin in PP is responsible for a decrease of >80% of the strain at break, ~30% of the tensile strength, and 25% of the material stiffness (Dias et al., 2019). Several approaches have been presented in the literature to address this matter. Among all, chemical modifications of lignin, such as alkylation (Sakai et al., 2018), esterification (Maldhure et al., 2010), and grafting with polyethylene glycol (Tanks et al., 2023), often in combination with the use of MAn-g-PP, have been extensively studied (Yeo et al., 2015; Dias et al., 2019). Conversely, very little work has been done on the use of alternative and more environment-friendly compatibilization strategies, not involving the use of wet-chemistry, e.g., through mechanical or physical methods (Iyer and Torkelson, 2015; Miao and Hamad, 2017).

Plasma-induced functionalization processes provide a versatile and viable tool for the straightforward physical modification of polymer surfaces (Lee et al., 2009). Due to the interaction with energetic particles, reactive free radicals can readily form on the surface of the material under treatment (Liston et al., 1993). A few works have investigated the effect of lignin powder treated by plasma in the presence of a functionalizing chemical (e.g., lactic acid) (Atz Dick et al., 2017), functionalizing gases (e.g., carbon dioxide, sulfur hexafluoride) (Zaitsev et al., 2018; Souza et al., 2019), or in inert or air atmosphere (Klarhöfer et al., 2010; Cao et al., 2020). Interestingly, a remarkable reduction in the concentration of hydroxyl functionalities was observed in lignin as a consequence of argon-plasma treatment (Zanini et al., 2005; Klarhöfer et al., 2010). In spite of these encouraging results, no work so far has focused on the effect of the incorporation of plasma-modified lignin into a polyolefin matrix on the chemical-physical, mechanical, and rheological properties of the resulting composite material.

To bridge this gap, in this work, commercial lignin obtained through the high-yield soda pulping method (Lobato-Peralta et al., 2021) was subjected to a novel plasma treatment to increase its compatibility with PP, ultimately investigating the effect of this compatibilization strategy on the properties of the PP-lignin blend. A gliding arc tornado (GAT) device was used for the first time to treat lignin, specially designed for processing powders in different gas atmospheres. The GAT device consists of a specific configuration of gliding arc plasma where the gas flux is used to create a vortex-tornado regime (Kalra et al., 2005; Barni et al., 2021). As reported recently, this GAT configuration is particularly suitable for treating powders without the need to deposit them in the form of a coating (e.g., by solvent casting) (Barni et al., 2021; 2022; 2023). Indeed, the tangentially injected gas generates the vortex flow in the discharge region while being capable of efficiently transporting the powders. This ensures an optimal interaction between the particles and the discharge gas phase, together with a much longer residence time in the plasma chamber than what is typically found under laminar flow (Kalra et al., 2005). Besides this, due to the high energy efficiency and strong reactivity towards powders and fluids, reactors operating in the gliding-arc regime exhibit significant potential for large-scale applications (Rabinovich et al., 2022).

The effect of this treatment on the lignin powder was assessed by electron paramagnetic resonance (EPR) spectroscopy, $^{31}$P-nuclear magnetic resonance ($^{31}$P NMR) spectroscopy, differential scanning calorimetry (DSC), and thermogravimetric analysis (TGA). In addition, PP/lignin blends were prepared by melt-blending in a twin-screw extruder via the incorporation of 5% (*w/w*), 10% (*w/w*), and 20% (*w/w*) of either plasma-treated or pristine lignin (the latter used as reference material). All the obtained blends were extensively characterized in terms of their thermal response, thermo-oxidative stability, morphology, viscoelastic behavior, and mechanical properties, also following a second extrusion process to mimic possible thermo-mechanical recycling conditions.

## 2. Materials and methods

### 2.1. Materials

Commercial soda lignin (SL) Protobind 1000 ($M_w$ = 8 300; $M_w$ / $M_n$ = 5.4) was supplied by Tanovis AG (Alpnach, Switzerland). This lignin originated from a non-woody source (i.e., wheat straw and Sarkanda grass (*Tripidium bengalense*)) and its average particle

size was 1–10 μm. Before undergoing the plasma treatment or being directly blended with PP, SL was dried overnight in a vacuum oven at 50 °C. The PP for blending was provided by SABIC® in the form of pellets and was characterized by a melt flow index of 25 and a density of 0.90 g/cm$^3$. Before extrusion, PP pellets were milled to powder by cryo-milling (Cimma-Morandotti S.P.A., Pavia, Italy) to ensure optimal pre-mixing with lignin.

### 2.2. Plasma treatment of lignin

The SL powder was treated in a specially designed GAT laboratory device as shown in Fig. S1 (Barni et al., 2021). The discharge chamber consisting of a Pyrex tube (about 60 cm$^3$ capacity) was closed at the backside by a Teflon cylinder cap through which the electrode wire (a three-turn molybdenum coil) was inserted. At the frontside, the tube was partially closed by a hollow stainless-steel disc, which constitutes the cathode of the system. A couple of Teflon hollow discs surrounding the Pyrex tube were also used for system sealing. Argon was injected in the chamber both tangentially, by two opposed channels excavated in the frontside Teflon disc, and axially through an inlet placed in the back cap. In this way, a reverse flow vortex was produced in the chamber spiraling downward along the Pyrex inner surface up to the Teflon backside cap, while a jet was formed along the axis exiting from the frontside central hole. To provide the power needed for the initiation of the plasma, a high-voltage direct current (DC) generator (SHV9000, Alintel, Italy) was employed (maximum 5 kV and 2 A, simultaneously). The discharge was operated in a spark regime, supplying the current intermittently (200 mA), so that an intermittent arc is generated and excessively high temperatures will be avoided. Lignin was allowed to enter the chamber using a powder injector consisting of a cylindrical Pyrex-glass container equipped with a lateral plunger able to carry a maximum of 300 mg of powder per batch. When argon gas was supplied at the pressure of 0.3 MPa, lignin was directly brought into the discharge chamber by the gas flow. The so-treated lignin powders exiting the chamber were then collected in a perforated metal tube internally coated with a rolled up polyester filter, placed at the front end.

### 2.3. Characterization of plasma-treated lignin

A series of characterization analysis were carried out on pristine SL before and immediately after plasma treatment (Plasma-SL) to assess potential modifications in the lignin functionalities and morphology.

Electron paramagnetic resonance (EPR) spectra were recorded to investigate the nature and abundance of radical species eventually formed in lignin samples upon plasma processing. Analysis was conducted at 298 K on a Bruker EMX spectrometer (USA) working at the X-band frequency, equipped with a variable temperature BVT 2000 unit (Bruker), by using a microwave power of 5 mW. According to the fundamental EPR resonance equation, the energy absorbed or emitted by an electron in a magnetic field $B_0$ can be expressed as Eq. (1):

$$h\nu = g\mu_B B_0 \tag{1}$$

where $h$ is the Planck constant ($6.62 \times 10^{-34}$ J/Hz), $\nu$ is the frequency (Hz), $g$ is a multiplicative dimensionless factor, also known as $g$-factor, which depends on the spin magnetic moment and angular momentum, and $\mu_B$ is the Bohr magneton ($9.274 \times 10^{-24}$ J/T) (Beckert et al., 2002). Experimentally, the $g$-factor (±0.001) was determined by Eq. (1) and using $\alpha,\alpha'$-diphenyl-$\beta$-picryl hydrazyl (DPPH) as standard. The concentration of paramagnetic species, expressed as the number of spins per gram of sample, was calculated with ± 10% accuracy by double integration of the resonance line and referring the area under the absorption curve to that of the standard Bruker weak pitch ($9.7 \times 10^{12}$ spins per cm with the accuracy of ±5%). All concentrations of paramagnetic species were normalized as a function of the sample weight (filling the EPR tube for 1 cm in height).

Quantitative $^{31}$P NMR spectroscopy was used to assess the type and concentration of hydroxyl and carboxyl functionalities in lignin samples. Spectra were recorded by inverse gate proton decoupling sequences on a Bruker Avance 500 spectrometer (USA) with 5 mm direct detection broadband probe-head, at 27 °C with 384 transients using 90° pulse flip angle with an acquisition time of 1 s and the relaxation delay of 5 s. Pristine SL and Plasma-SL were prepared for the analysis according to a procedure described in the literature (Balakshin and Capanema, 2015). The integration regions were $150.7 \times 10^{-6} - 150.6 \times 10^{-6}$ (internal standard), $148.0 \times 10^{-6} - 144.5 \times 10^{-6}$ (aliphatic hydroxyls), $143.0 \times 10^{-6} - 136.2 \times 10^{-6}$ (phenolic hydroxyls), and $134.8 \times 10^{-6} - 132.6 \times 10^{-6}$ (carboxylic groups).

Differential scanning calorimetry (DSC) analysis was employed to determine how thermal transitions in SL lignin were affected by plasma treatment. Measurements were carried out with 10–15 mg samples using a Mettler-Toledo DSC 823e instrument (Switzerland). Three runs (heating-cooling-heating) were performed from 25 to 150 °C (to erase previous thermal history and remove possible physically adsorbed water), from 150 to 25 °C, and from 25 to 200 °C, at a scan rate of 20 °C/min under nitrogen flux. The glass transition temperature ($T_g$) of the samples was evaluated as the inflection point in the second heating run.

Thermogravimetric analysis (TGA) was conducted on ~10 mg of lignin samples to study their thermo-oxidative stability before and after Ar-plasma treatment, using a Q500 TGA system (TA Instruments, USA) from ambient temperature to 800 °C at a scan rate of 20 °C/min in air.

The morphology of pristine and plasma-treated lignin powder was analyzed using scanning electron microscopy (SEM) with a Zeiss EVO 50 microscope (Germany; Fig. S2).

### 2.4. Production of PP/lignin blends and materials

Before melt-blending, PP in powder form was manually premixed with 5% (*w/w*), 10% (*w/w*), and 20% (*w/w*) of pristine or plasma-treated SL in polyethylene bags, to ensure effective solid-state dispersion. Then, PP/lignin blends were prepared in a Process

**Table 1**
Twin-screw extruder and injection molding screw profile temperatures used for processing of PP and PP/lignin blends.

| Item | | Temperature ( °C) |
|---|---|---|
| Extruder zone | I | 170 |
| | II | 170 |
| | III | 180 |
| | IV | 185 |
| | V | 185 |
| | VI | 180 |
| | VII | 170 |
| | Die | 170 |
| Injection screw zone | I | 205 |
| | II | 205 |
| | III | 215 |
| | IV | 210 |
| | Die | 210 |

11 twin-screw extruder by Thermo Fisher Scientific (screw diameter = 11 mm) at 75 r/min, according to the temperature profile reported in Table 1, and at a constant feeding rate controlled by a volumetric hopper. About 60 g of the compounds for each blend were prepared. For comparative purposes, neat PP was also extruded in the same conditions.

For mechanical testing of PP/lignin blends, the extruded filaments were reduced in pellets of 2–3 mm by cryo-milling and used to produce A12-type dumbbell-shaped specimens by injection molding according to EN ISO 20,753:2018 (Plastics-test specimens, Switzerland). A BOY 25E injection molding machine was used, with the temperature profile reported in Table 1, a shot size of 5 $cm^3$, an injection pressure of 5 MPa, a packing pressure of 2.5 MPa, and a cooling time of 15 s.

In addition, to evaluate the extent of retention of mechanical properties of the PP/lignin materials following reprocessing (mechanical recycling), pure PP and 5% (*w*/*w*) PP/lignin blend formulations (with either pristine or plasma-treated SL) were subjected to two twin-screw extrusion cycles before undergoing injection molding and being mechanically tested.

### 2.5. Characterization of PP/lignin blends

Thermal transitions and crystallinity degree of the obtained PP/lignin blends were determined by DSC analysis. Three runs were performed: from 25 to 200 °C, from 200 to –50 °C, and from –50 to 250 °C at 10 °C/min. The temperature and the enthalpy associated with the melting process were considered from the second heating ramp, which excluded the effect of previous thermo-mechanical history (i.e., extrusion and injection molding). The crystallinity degree ($\chi$) of the blends was determined according to Eq. (2):

$$\chi = \frac{\Delta H_f^{obs}}{(1-\varphi)\times \Delta H_f^0} \times 100\% \tag{2}$$

where $\Delta H_f^{obs}$ corresponds to the measured heat of fusion of the material under study, $\varphi$ is the weight fraction of PP in the blends and $\Delta H_f^0$ is the fusion heat of 100% crystalline PP, i.e., 207.1 J/g (Lima et al., 2002; Novais et al., 2012).

The TGA was carried out on the ~15 mg samples to study their thermo-oxidative stability, using a Q500 TGA system (TA Instruments), from ambient temperature to 800 °C, at a scan rate of 20 °C/min, in air.

Rheological tests were performed with a TA instruments Discovery HR-2 rheometer (USA) equipped with a 25 mm plate-plate geometry at 190 °C (this temperature was selected as it approximates the processing temperatures used during extrusion/injection molding). The thickness of the tested samples was around 2 mm. Shear viscosity as a function of the shear rate of the blends was measured by maintaining a constant gap of 500 $\mu$m and applying a maximum normal stress of 5 kPa.

To determine the linear viscoelastic region (LVR) of the materials, strain sweep tests were conducted by varying the oscillation strain amplitude from 0.05% to 5% at 1 Hz. Dynamic frequency sweep measurements were then carried out to evaluate the relaxation time of the blends by increasing the oscillation frequency from 1 to 100 Hz by applying a maximum deformation of 1% according to LVR results (Fig. S7).

The relaxation process of a polymer melt was typically considered as the relaxation phenomenon occurring in the long-range time scale (i.e., the terminal region in the viscoelastic spectrum) (Elmoumni et al., 2003). In the case of polymers with sufficiently narrow molecular weight distribution, the longest relaxation time ($\lambda_{max}$) could be defined as Eq. (3) (Carri and Winter, 1997):

$$\lambda_{max} = \alpha \frac{1}{\omega_c} \tag{3}$$

where $\alpha$ is a polymer-specific constant, $\omega_c$ is the storage modulus ($G'$) and the loss modulus ($G''$) crossover frequency. In this work, a representative relaxation time ($\lambda_r$) for the different materials was reported and calculated as Eq. (4) (Elmoumni et al., 2003):

$$\lambda_r \approx \frac{1}{\omega_c} \tag{4}$$

Uniaxial tensile tests were performed according to EN ISO 527-1:2019 (Plastics-determination of tensile properties, Switzerland) on dumbbell-shaped specimens obtained by injection molding using a Zwick/Roell BT-FR010TH.A50 dynamometer equipped with a 10 kN load cell. After reaching 0.8% of deformation with an initial step of 1 mm/min, the tests were carried out under displacement control at a fixed displacement rate of 5 mm/min to allow for accurate calculation of the elastic modulus in the strain interval of 0.05%–0.25%. Deformation was measured using a long-stroke extensometer. For each sample, tensile elastic modulus ($E_t$), maximum stress at yield ($\sigma_y$), strain at yield ($\varepsilon_y$), and strain at break ($\varepsilon_b$) were evaluated following the above-mentioned standard. The theoretical elastic modulus ($E_{HT}$) of all the PP/lignin blends was estimated by the Halpin-Tsai model, according to Eqs. (5) and (6) (Halpin, 1969; Zare, 2016):

$$E_{HT} = E_m \times \frac{1 + \eta\xi\varphi_f}{1 - \xi\varphi_f} \tag{5}$$

$$\eta = \frac{\frac{E_f}{E_m} - 1}{\frac{E_f}{E_m} + \xi} \tag{6}$$

where $E_f$ and $E_m$ are the Young's modulus of the filler and the matrix, respectively, $\varphi_f$ is the volume fraction of the filler, $\xi$ is the aspect-ratio of the lignin particles, and $\eta$ corresponds to the aspect ratio correction factor. Values for lignin were assumed to be $E_f = 6.7$ GPa and $\xi = 1$ (Tanks et al., 2023).

After the second extrusion step, the retention rate ($R$) for each measured mechanical property ($M$) was expressed according to Eq. (7):

$$R = \left(1 - \frac{M_1 - M_2}{M_1}\right) \times 100\% \tag{7}$$

where $M_1$ corresponds to the property measured after the first extrusion run and $M_2$ is the same property measured following the second extrusion run.

The SEM was used to investigate the morphology of the samples, the lignin-PP interface, and the lignin distribution in PP matrix. Each specimen was cryo-fractured after cooling in liquid nitrogen. The cross section was thus obtained and then metalized with Au to make it conductive and analyzed by a Zeiss EVO 50 (Germany) scanning electron microscope.

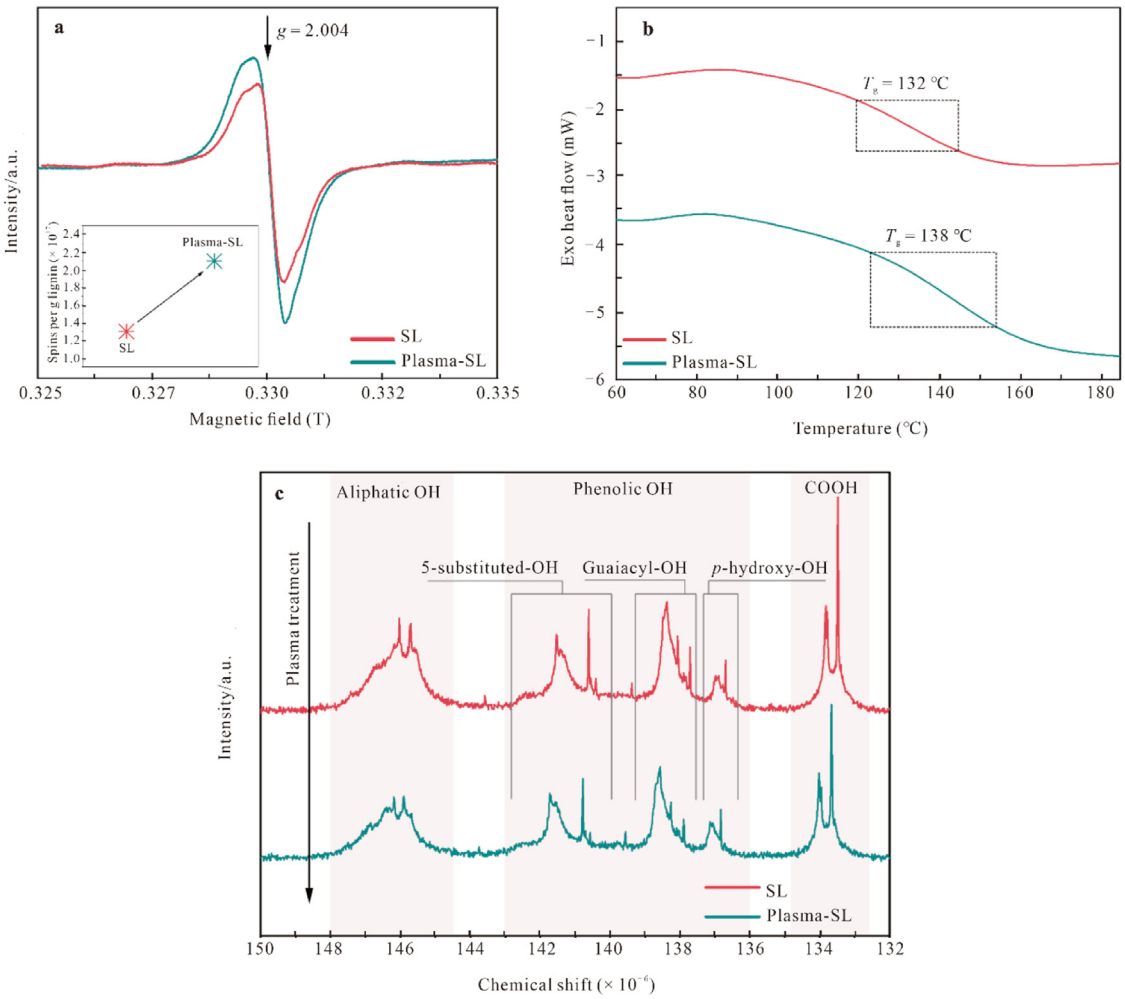
## 3. Results and discussion

### 3.1. Plasma treatment-induced modifications of lignin

Following the Ar-plasma treatment in the GAT process chamber, lignin was recovered from the collector filter of the device (Fig. S1c) and characterized. To investigate treatment-related changes in the lignin structure, pristine SL was also considered as a reference.

The formation of free radicals in lignin samples upon plasma treatment was monitored by EPR spectroscopy. In particular, the nature of the paramagnetic species and their concentration in SL and Plasma-SL were determined. In Fig. 1a, the EPR spectra of SL and Plasma-SL showed the co-presence of two signals with high signal-to-noise ratios, both signals were centered at a $g$-factor of 2.004 and attributable to phenoxy radicals (Hon, 1992). The two signals detected both before and after the plasma treatment were characterized by different line widths, i.e., the difference between the position of the signal maximum and minimum in the magnetic field ($(5.0 \pm 0.5) \times 10^{-4}$ and $(9.8 \pm 0.5) \times 10^{-4}$ T, respectively). This feature could be explained by considering the substantial heterogeneity of lignin radical sites and the possible polar interactions occurring among spatially-close radicals (Weil and Bolton, 2006). As displayed in the inset of Fig. 1a, the concentration of phenoxy radicals increased by >60% (from $1.3 \times 10^{17}$ to $2.1 \times 10^{17}$ of spins per gram of lignin) as a result of the plasma treatment. The formation of new phenoxy radical species in lignin could result from dehydrogenation reactions induced by interactions of functional groups with activated radicals (Fig. 2a) (Patil and Argyropoulos, 2017), and from cleavage of $\beta$-O-4 aryl ether intermonomeric linkages caused by plasma-charged particles (Fig. 2b) (Zanini et al., 2008; Cao et al., 2020).

More in-depth information about the functionalities of post-treatment lignin was provided by $^{31}$P NMR. Lignin phosphitylation allows for the determination of the abundance of aliphatic hydroxyl groups, aromatic hydroxyl groups (i.e., phenolic 5-substituted-OH, guaiacyl-OH, $p$-hydroxy-OH), and aliphatic carboxylic acids in the lignin structure. In Fig. 1c, $^{31}$P NMR spectra of SL and Plasma-SL were shown, together with the corresponding regions of integration, while in Table 2 the resulting molar concentration of each functional group was reported. As a consequence of plasma treatment, a general reduction of hydroxyl functionalities with respect to the pristine material was observed. More in detail, aliphatic hydroxyls, phenolic hydroxyls, and carboxylic acids were found to decrease by 39%, 30%, and 32%, respectively. This effect, partially observed in previous studies (Zanini et al., 2008; Klarhöfer et al., 2010), can be explained by considering that plasma species preferentially interacted with highly electronegative oxygen-containing functional groups. In this context, aliphatic hydroxyls could be cleaved, while new double bonds were formed between $\alpha$ and $\beta$ carbons, leading to increased conjugation and concurrent decrease in aliphatic –OH concentration (Fig. 2c) (Moliton et al., 1996; Klarhöfer et al., 2010). The reduction of free phenolic hydroxyl moieties was instead likely associated with the formation of phenoxy radicals, as indicated by EPR analysis, and subsequent re-formation of different intermonomeric bonds due to radicals coupling (Zanini et al., 2008). The most notably affected units were the 5-substituted phenolic hydroxyls (33% decrease), which account




$T_g$, glass transition temperature; $g$, $g$-factor.

**Fig. 1.** (a) Electron paramagnetic resonance (EPR) results, (b) differential scanning calorimetry (DSC) traces, and (c) $^{31}$P-nuclear magnetic resonance (NMR) spectra of pristine soda lignin (SL) and soda lignin treated by plasma (Plasma-SL).

**Table 2**
Molar concentration of aliphatic OH, 5-substituted OH, guaiacyl OH, *p*-hydroxy OH, total phenolic OH and COOH (mmol/g).

| Lignin | Aliphatic –OH | 5-substituted –OH | Guaiacyl –OH | *p*-hydroxy –OH | Total phenolic –OH | –COOH |
|---|---|---|---|---|---|---|
| SL | 2.34 | 1.64 | 1.44 | 0.46 | 3.54 | 1.07 |
| Plasma-SL | 1.42 | 1.09 | 1.03 | 0.35 | 2.47 | 0.72 |

Notes: SL, soda lignin; Plasma-SL, soda lignin treated by plasma.

for both syringyl hydroxyl and condensed 5-substituted phenolics (Constant et al., 2016). These latter included also phenolic units connected by 5–5′ bond, which could eventually recombine (upon formation of phenoxy radicals) resulting in the formation of new 5–5′-O-4 connections (Fig. 2d) (Zanini et al., 2008). In contrast to what is observed for aliphatic and phenolic hydroxyls, the decrease in carboxyl-type functionalities following plasma treatment has never been previously reported in the literature. The significant reduction in carboxylic acids experienced in this study might be attributed to the cleavage of carboxyl groups and the subsequent formation of new double bonds, similar to the case of aliphatic hydroxyl moieties (Moliton et al., 1996). As opposed to the mild oxidative phenomena observed in previous reports (Zanini et al., 2008; Klarhöfer et al., 2010; Zaitsev et al., 2018; Cao et al., 2020), this result might be ascribed to the successful application of the GAT configuration, which ensured excellent mixing of the lignin powders with the inert gas, avoiding any possible reaction with oxygen.

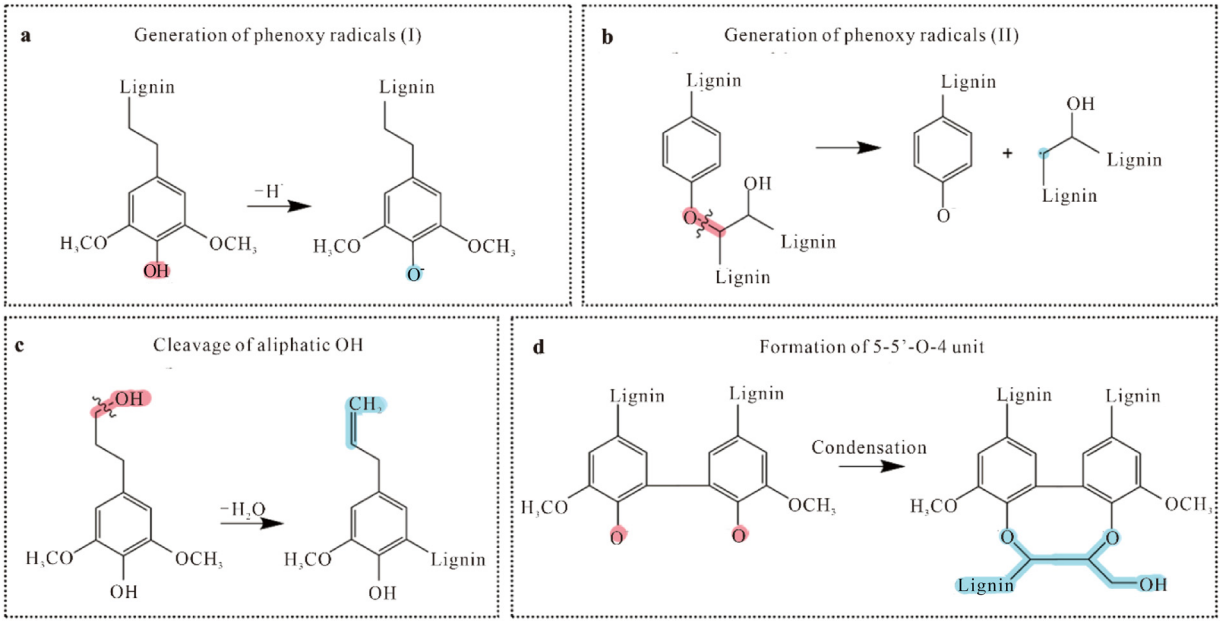



**Fig. 2.** Possible reaction mechanisms occurring during gliding arc tornado (GAT) plasma treatment of lignin in argon atmosphere (Functional groups/bonds present in the pristine lignin were marked in red, while the new functional groups/bonds formed after the treatment were highlighted in blue.).

To further assess the effect of plasma treatment on thermal transitions of lignin, DSC analysis was also carried out on both SL and Plasma-SL (Fig. 1b). As the first consideration, it was noteworthy that the GAT configuration enabled homogeneous treatment of the lignin sample with no formation of core-shell structures, thus resulting in a single $T_g$. Interestingly, the value for $T_g$ in Plasma-SL is 6 °C higher than that of the untreated SL, in contrast with the increased macromolecular mobility expected as a result of the significant decrease in polar functionalities experienced after the plasma treatment (reduction of hydrogen bonding interactions between macromolecular chains). On the contrary, this slight increase in $T_g$ for Plasma-SL might be the possible formation of new intermonomeric linkages between lignin molecules, which ultimately led to an increase in molecular weight and a more condensed lignin network (Zaitsev et al., 2018). The presence of a more condensed structure and the simultaneous decrease in $\beta$-O-4 linkages was further supported by the enhanced thermo-oxidative stability of Plasma-SL. Indeed, Plasma-SL exhibited a slightly lower weight loss at 150–300 °C (17.3% and 14.9% for SL and Plasma-SL, respectively), which was typically associated with the breakage of $\alpha$- and $\beta$-aryl-alkyl-ether linkages (Fig. S6 and Table S1) (Domínguez et al., 2008; Scarica et al., 2018). Additionally, the derivative of the gravimetric curve indicated that the main thermal degradation event for lignin, associated with the rupture of intramolecular carbon-carbon linkages (at ~500 °C) (Domínguez et al., 2008), was broader and shifted to higher temperatures in the case of plasma-treated lignin.

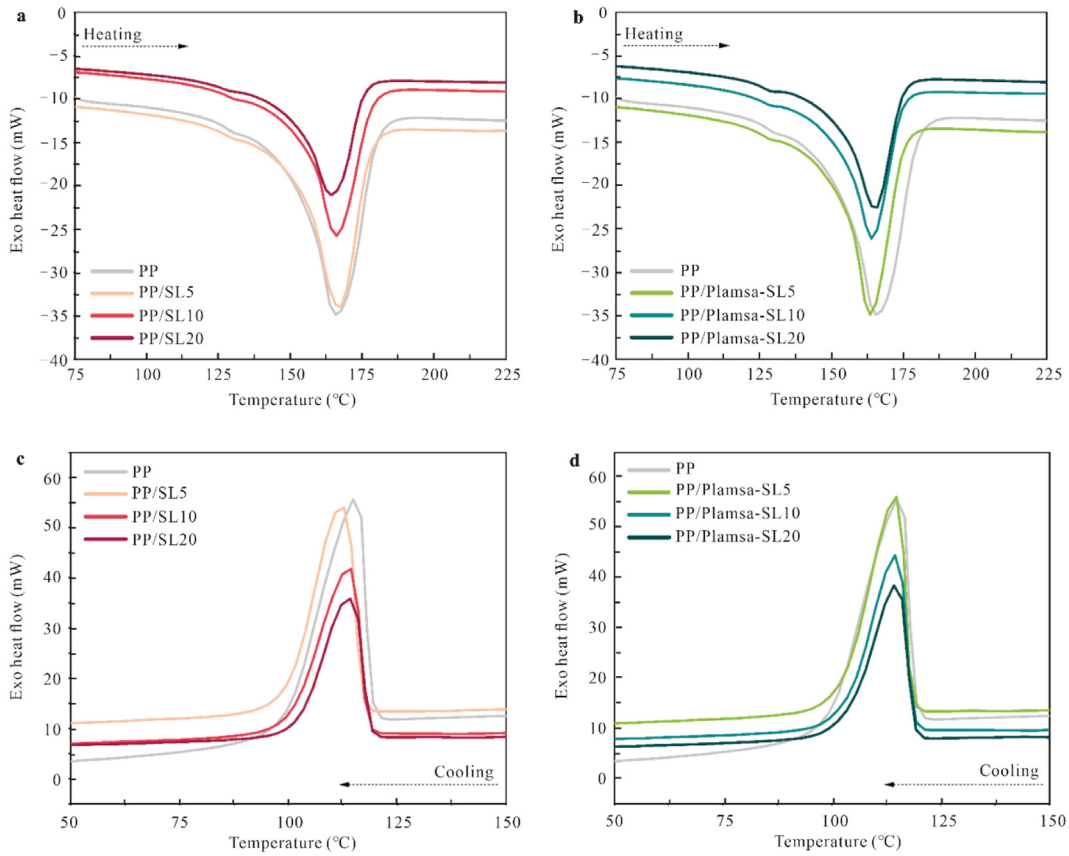
In brief, plasma treatment resulted in the formation of new meta-stable phenoxy radical species both on the surface and within the bulk of SL. The eventual recombination of lignin monomeric units into more condensed structures, in addition to the cleavage of some of the aliphatic hydroxyl and carboxyl groups, led to an overall reduction of hydroxyl and carboxyl functionalities and a more condensed lignin architecture. The observed increase in the concentration of active sites along with the reduction in polar functionalities in plasma-treated lignin, in conjunction with its enhanced thermo-oxidative stability derived from its highly condensed structure, lay the groundwork for the successful preparation of homogeneous PP/lignin blends.

### *3.2. Thermal and thermo-oxidative properties of PP/lignin blends*

To assess the potential of plasma treatment on lignin in thermoplastic blends, Plasma-SL was compounded with PP at various weight percentages (5%, 10%, and 20%).

The non-isothermal melting and crystallization behavior of all the PP/lignin blends were studied by DSC (Fig. 3 and Table 3), monitoring the temperature and enthalpy associated with the melting process ($T_m$ and $\Delta H_m$, respectively), the degree of crystallinity ($\chi_c$,), and the temperature and enthalpy associated with crystallization ($T_c$ and $\Delta H_c$, respectively).

In all the analyzed materials, a single melting peak was consistently observed at around 165 °C with no significant temperature difference noted in the blends containing lignin. This temperature corresponded to the melting point of the $\alpha$-crystalline phase, characteristic of isotactic PP (Lotz, 1998). Notably, even with 20% lignin, no additional melting peaks associated with secondary crystalline phases (i.e., $\beta$-phase) were detected. This suggested an effective melt blending, resulting in highly homogeneous materials with no phase segregation (see also SEM images in Figs. S4–S5). Similarly, lignin was not found to affect the type of crystallites formed




PP, polypropylene; PP/SL5, PP with 5% (*w/w*) SL; PP/SL10, PP with 10% (*w/w*) SL; PP/SL20, PP with 20% (*w/w*) SL; PP/Plasma-SL5, PP with 5% (*w/w*) Plasma-SL; PP/Plasma-SL10, PP with 10% (*w/w*) Plasma-SL; PP/Plasma-SL20, PP with 20% (*w/w*) Plasma-SL.

**Fig. 3.** The DSC traces associated with the second heating cycle of (a) PP and PP/lignin blends based on pristine SL and (b) PP and PP/lignin blends based on Plasma-SL; The DSC traces during the cooling step of (c) PP and PP/lignin blends based on pristine SL and (d) PP and PP/lignin blends based on Plasma-SL.

**Table 3**
Melting temperature ($T_m$), enthalpy of melting ($\Delta H_m$), crystallinity degree ($\chi_c$), crystallization temperature ($T_c$), and enthalpy of crystallization ($\Delta H_c$) of pure PP and PP/lignin blends.

| Sample | $T_m$ (°C) | $\Delta H_m$ (J/g) | $\chi_c$ (%) | $T_c$ (°C) | $\Delta H_c$ (J/g) |
|---|---|---|---|---|---|
| PP | 165.4 | 108.6 | 52.4 | 114.8 | 109.5 |
| PP/SL5 | 167.1 | 103.5 | 52.6 | 112.7 | 106.1 |
| PP/SL10 | 166.0 | 100.5 | 51.0 | 114.3 | 103.9 |
| PP/SL20 | 164.2 | 97.2 | 58.7 | 114.1 | 98.7 |
| PP/Plasma-SL5 | 167.8 | 103.3 | 52.5 | 114.9 | 106.1 |
| PP/Plasma-SL10 | 165.8 | 102.2 | 54.8 | 114.4 | 105.7 |
| PP/Plasma-SL20 | 164.2 | 98.9 | 59.7 | 114.3 | 100.3 |

Notes: PP, polypropylene; PP/SL5, PP with 5% (*w/w*) SL; PP/SL10, PP with 10% (*w/w*) SL; PP/SL20, PP with 20% (*w/w*) SL; PP/Plasma-SL5, PP with 5% (*w/w*) Plasma-SL; PP/Plasma-SL10, PP with 10% (*w/w*) Plasma-SL; PP/Plasma-SL20, PP with 20% (*w/w*) Plasma-SL.

by the PP fraction. Considering $T_c$, analogous conclusions could be drawn. Indeed, the crystallization temperature was always found at around 114 °C, thus indicating a negligible difference in the degree of undercooling (i.e., driving force for crystallization) between the reference PP and the lignin-blends (Wang et al., 2024). As expected, both $\Delta H_m$ and $\Delta H_c$ were found to be lower for PP/lignin blends compared to neat PP and progressively decreased as lignin content increased due to the lower fraction of material able to crystallize (i.e., PP). Conversely, the degree of crystallinity ($\chi_c$) (calculated based only on the PP amount within the formulation) was found to systematically increase with the lignin load and to be slightly higher in the case of plasma-modified PP/lignin blends.

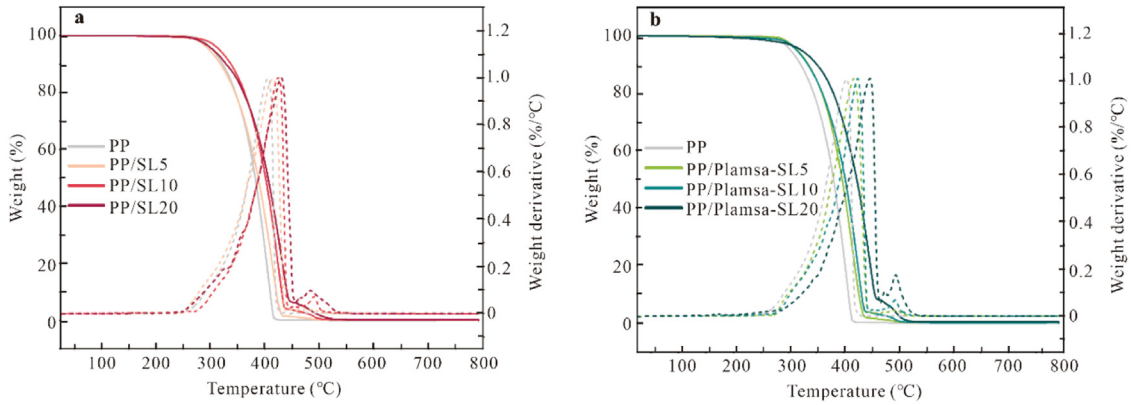



**Fig. 4.** Thermogravimetric mass loss traces and thermogravimetric derivative curves (solid line: weight; dash line: weight derivative). (a) PP and PP/lignin blends based on pristine SL; (b) PP and PP/lignin blends based on plasma-treated SL.

For instance, $\chi_c$ increases from 52.4% for neat PP to 58.7% and 59.7% for PP/SL20 (PP with 20% (*w/w*) SL) and PP/Plasma-SL20 (PP with 20% (*w/w*) Plasma-SL), respectively. This trend could be justified considering the lignin capability to foster crystallization of the PP matrix acting as a nucleation site, particularly in the case of Plasma-SL (Lu et al., 2016; Tanks et al., 2023). Such behavior was attributed to a refined interaction between lignin and PP, which minimized the reduction of PP chain mobility, facilitating their packing into a more regular structure (i.e., $\alpha$-crystalline phase) (Wang et al., 2024).

To assess the thermo-oxidative stability of the different blends, TGA measurements were performed in an air atmosphere. The thermogravimetric mass loss traces (TG), together with the thermogravimetric derivative curves (DTG), as a function of the temperature for all materials, were shown in Fig. 4. The thermo-oxidative degradation profile of neat PP was characterized by a single-step event initiating at around 300 °C and reaching the maximum weight loss at 405 °C (Table S2). This mass loss was typically associated with the onset of the formation of free radical species at the tertiary carbon in the polymer backbone (Grassie, 1983). The addition of lignin (both SL and Plasma-SL) led to a remarkable increase in the thermo-oxidative stability of the PP matrix as evidenced by the shift of the TG curves and the corresponding DTG peaks to higher temperatures. This response was found to be progressively more evident for increasing lignin content in the material and could be associated with the radical scavenging activity of the hindered phenolic units constituting the lignin macromolecular structure. In particular, the presence of substituents in both ortho positions of the syringyl phenolic units (abundant in soda lignin) enhanced the free radical scavenging ability of lignin due to increased steric hindrance (Gadioli et al., 2016). Interestingly, the beneficial effect on the thermo-oxidative stability of PP was even more pronounced in compounds based on plasma-treated lignin (PP/Plasma-SL), in which the mass loss onset and the maximum weight loss were found at higher temperatures than in the case of untreated PP/SL blends (Table S2). These results could be explained by two distinct factors. First, the well-known antioxidant effect of lignin towards PP was generally found to be more effective when its compatibility/interaction with the polyolefin was enhanced by a lower concentration of hydroxyl-type moieties in lignin (Pouteau et al., 2003). Second, the intrinsically higher thermo-oxidative stability of plasma-treated lignin (see Section 3.1) might also positively affect the thermal response of PP/Plasma-SL blends. In support of this, the DTG plot revealed a secondary high-temperature peak ($T > 450$ °C), which became more pronounced with increasing lignin content. This peak was indicative of the primary thermal degradation event in lignin (Fig. S6) and consistently appeared at higher temperatures in PP/Plasma-SL blends compared to PP/SL blends.

Overall, plasma treatment of lignin proved to have a beneficial effect on the thermal properties of PP/lignin blends. Indeed, the reduced concentration in polar functionalities (i.e., hydroxyl and carboxyl groups) was responsible for an enhanced interfacial affinity with the polyolefin matrix. This effect could promote the formation of a homogeneous crystalline phase, while ensuring an inherently higher thermo-oxidative stability of plasma-treated lignin, ultimately yielding superior thermo-oxidative resistance to the PP blends.

### *3.3. Rheological behavior of PP/lignin blends*

To investigate the behavior of the polymer melting under processing conditions and gain a deeper understanding of the interactions of pristine and treated lignin particles with the PP matrix, the rheological response of PP/lignin blends and neat PP was assessed by rotational rheometry at 190 °C.

As illustrated in Fig. 5, all the analyzed samples exhibited a typical shear-thinning behavior that became much more pronounced with the increased lignin content. Interestingly, while the zero-shear viscosity was found to be comparable in all the materials (approximately 1 000 Pa·s), PP/lignin blends showed a markedly different behavior at higher shear rates compared to neat PP. Indeed, while a single Newtonian plateau was observed in PP up to a shear rate of ~10 per second followed by the characteristic shear-thinning response of polymer melts (Barnes, 2000), two distinct plateaus could be clearly distinguished in all PP/lignin blends.

A first Newtonian plateau occurred for low shear rates (< 0.1 per second), resulting from molecular and chain interactions (Barnes, 2000). For shear rates between 0.1 and 1 per second, a shear thinning behavior associated with the breakdown and reorganization of the lignin aggregates was observed (Jalaee et al., 2024). At the shear rate of ~1 per second, the onset of a secondary

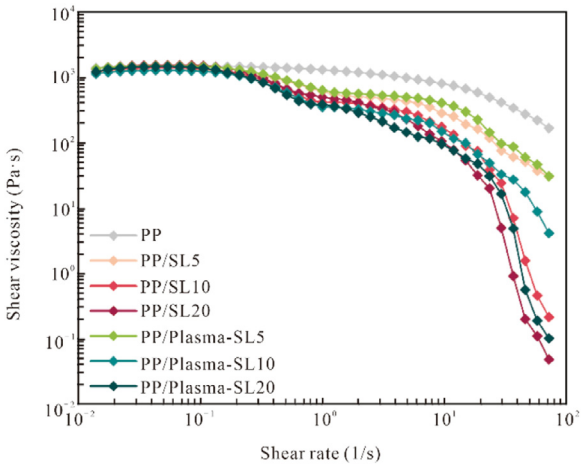



**Fig. 5.** Viscosity curves of PP and PP/lignin blends at 190 °C.

plateau was detected, likely caused by lignin particles hindering the relative motion of polymer chains (Wang et al., 2024). For higher shear rates (> 10 per second for blends with 5% lignin content; > 2 per second for blends containing 10% and 20% of lignin), a marked shear-thinning behavior was again observed with the viscosity decrease becoming more significant as lignin content increased. The dramatic drop in the shear viscosity observed for PP/lignin blends based on 10% or 20% of lignin was likely to be associated with reduced interaction between PP matrix and lignin particles, which increased free space between macromolecules and favored material flow as previously reported, in the presence of other types of fillers (e.g., mineral) (Barnes, 2000). Notably, across the entire range of shear rates examined, especially at higher shear rates, the viscosity of the blends incorporating treated lignin appeared to be higher than that of blends with pristine lignin. This behavior, recorded at all lignin loadings, suggested stronger intermolecular interactions (i.e., enhanced interfacial bonding) between PP and Plasma-SL compared to untreated SL (Abdelwahab et al., 2019; Tian et al., 2022), contributing to a reduction in intermolecular free volume and an increase in resistance to flow (Moan et al., 2000). Such a more accentuated shear-thinning response found in lignin-containing blends might positively affect the processability of the materials. Indeed, a lower melt viscosity registered at shear rates typical of processing technologies, such as injection molding (> 100 per second), implied lower operating torques, ultimately reducing energy consumption (Abdelwahab et al., 2019; Jalaee et al., 2024). At the same time, plasma treatment ensured an enhanced interaction between the incorporated lignin and the polymer matrix, further validating the findings discussed in Section 3.2.

During melt processing, polymers might undergo degradative phenomena resulting from high-temperature/high-shear-stress conditions. As mentioned in the previous section, thermo-oxidative degradation of PP typically occured by chain scission, which led to a reduction of the molecular weight of the polymer (Grassie, 1983). To elucidate the role of lignin acting as a thermal stabilizer for PP, dynamic frequency sweep analysis was performed at 190 °C monitoring the storage modulus ($G'$) and the loss modulus ($G''$) at increasing angular frequency. As recalled in Eq. (4), the crossover frequency ($\omega_c$) at which $G'$ and $G''$ intersect was inversely proportional to the terminal relaxation time ($\lambda_r$) of a polymer. In particular, $\lambda_r$, the time necessary for elastic stresses to relax through microstructural rearrangements and be converted into viscous ones, increased with the molecular weight (Vega et al., 2004), thus anticipating longer relaxation times (i.e., lower $\omega_c$ values) for higher molecular weight polymers.

Figs. 6a–b show $G'$ and $G''$ as a function of angular frequency in isothermal conditions (190 °C) at a fixed strain amplitude of 1% for neat PP and all PP/lignin blends. The observed $G'$-$G''$ crossover frequency ($\omega_c$) and the corresponding relaxation time ($\lambda_r$) for each material were reported in Fig. 6c. As expected, the low-frequency region of all the materials displayed a viscous liquid-like behavior with $G'' > G'$, while $G'$ became larger than $G''$ at high frequencies as a consequence of the prevailing elastic solid-like response. Both $G'$ and $G''$ were found to be lower for PP/lignin blends compared to neat PP across the entire frequency region, irrespective of the lignin type and content. This result was typically associated with the substantial lack of miscibility between lignin particles and PP (Wang et al., 2024). Interestingly, the characteristic crossover frequency ($\omega_c$) in neat PP was found at higher values than in blends containing 5% ($w/w$) and 10% ($w/w$) of lignin, with PP/Plasma-SL systems exhibiting the lowest $\omega_c$ values. These considerations entailed longer relaxation times ($\lambda_r$) in PP/lignin blends concerning neat PP, as a result of two complementary effects: on one end, the presence of lignin in these systems might physically hinder the relaxation processes of polymer chains (Wang et al., 2024); on the other end, the antioxidant activity of lignin might help to prevent PP degradation and its subsequent molecular weight reduction. Notably, the relaxation time of blends incorporating plasma-treated lignin was longer than in the corresponding untreated counterpart (at 5% ($w/w$) and 10% ($w/w$) loading), it was likely attributed to a more effective antioxidant activity of Plasma-SL originating from its increased interactions with the PP matrix, as previously discussed (see TGA analysis in Fig. 4). The substantial reduction in the relaxation time (higher $\omega_c$) observed in PP/SL20 and PP/Plasma-SL20 might be associated with the high lignin load, yielding poor PP/lignin interfacial adhesion and likely resulting in increased free volume, higher macromolecular mobility, and accelerated relaxation processes. This observation was in line with the lower viscosity observed in high-lignin-content blends as discussed previously (Fig. 5).

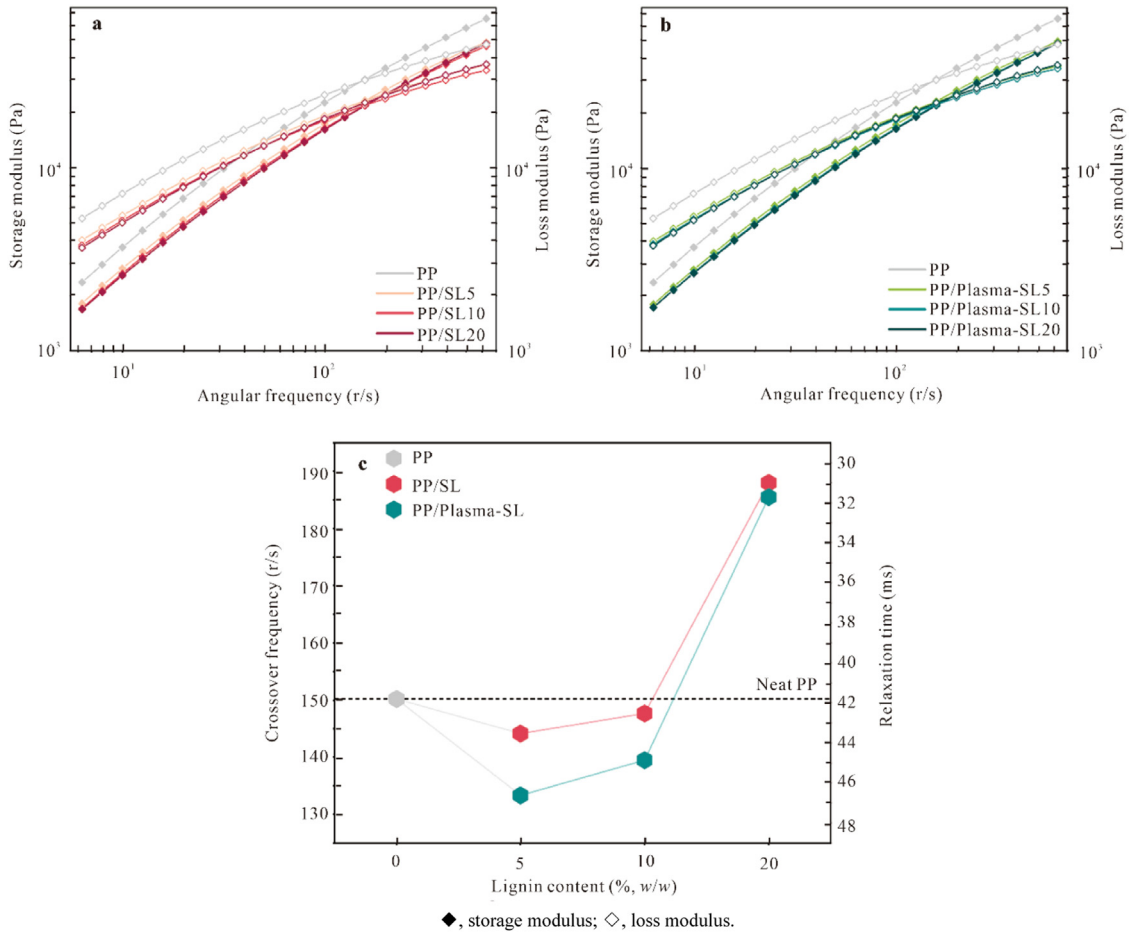



**Fig. 6.** Dynamic frequency sweep tests (190 °C, 1% strain amplitude). Storage modulus ($G'$) and loss modulus ($G''$) as a function of angular frequency of (a) PP and PP/lignin blends based on pristine SL, and (b) PP and PP/lignin blends based on plasma-treated SL; (c) The $G'$-$G''$ crossover frequency and corresponding relaxation time as a function of lignin content.

### *3.4. Mechanical performance and reprocessability of PP/lignin blends*

To assess the influence of lignin loading and plasma-treatment on the mechanical response of PP/lignin blends, uniaxial tensile tests were performed on neat PP (as reference) and blends incorporating untreated (SL) or plasma-treated (Plasma-SL) lignin at 5%, 10% and 20%. For all materials, tensile modulus ($E_t$), yield strength ($\sigma_y$), and strain at break ($\varepsilon_b$) were displayed in Fig. 7, while yield strain ($\varepsilon_y$) and representative stress-strain curves were reported in Figs. S9 and S10. Both PP and PP/lignin blends exhibited an elastic-plastic behavior characterized by a distinct yield point and a plastic region that shortened as the lignin content increased (Fig. S10).

As observed in Fig. 7a, when blended with PP, lignin behaved as a well-dispersed and rigid filler, resulting in progressively increased tensile modulus with lignin content up to 10% (*w/w*) (Iyer and Torkelson, 2015; Dias et al., 2019; Tanks et al., 2023; Wang et al., 2024), irrespective of the plasma treatment. The incorporation of higher lignin loadings (20%, *w/w*) did not lead to a further increase in $E_t$. This trend could be explained by considering the cross-section morphology of 20% (*w/w*) PP/lignin blends, in which part of the lignin easily detached from the polymer matrix, likely contributing to the reduction in the measured stiffness (Figs. S4 and S5). Interestingly, the experimental $E_t$ values measured in 5% (*w/w*) and 10% (*w/w*) PP/lignin systems (both pristine and plasma-treated lignin) significantly exceeded those predicted by the Halpin-Tsai model, while good match between theoretical and experimental values was found in the case of 20% (*w/w*) PP/lignin blends (Fig. 7b). This result provided further evidence of an efficient PP/lignin mixing process during extrusion for low-to-moderate lignin contents, yielding an optimal dispersion of lignin within the polymer matrix. The incorporation of lignin led to a slight decrease (12%–15%) in the yield strength ($\sigma_y$) (Fig. 7c) of all the blends compared to neat PP, irrespective of the lignin type (pristine, plasma-treated) and content. This trend was often reported in the reference literature, and it was typically associated with the limited compatibility and modest adhesion between lignin and the polymer matrix, which led to a reduction of the particle-matrix stress transfer (Pouteau et al., 2004; Luo et al., 2017; Abdelwahab et al., 2019; Dias et al., 2019; Wang et al., 2024). Nonetheless, the blends including plasma-treated lignin showed slightly

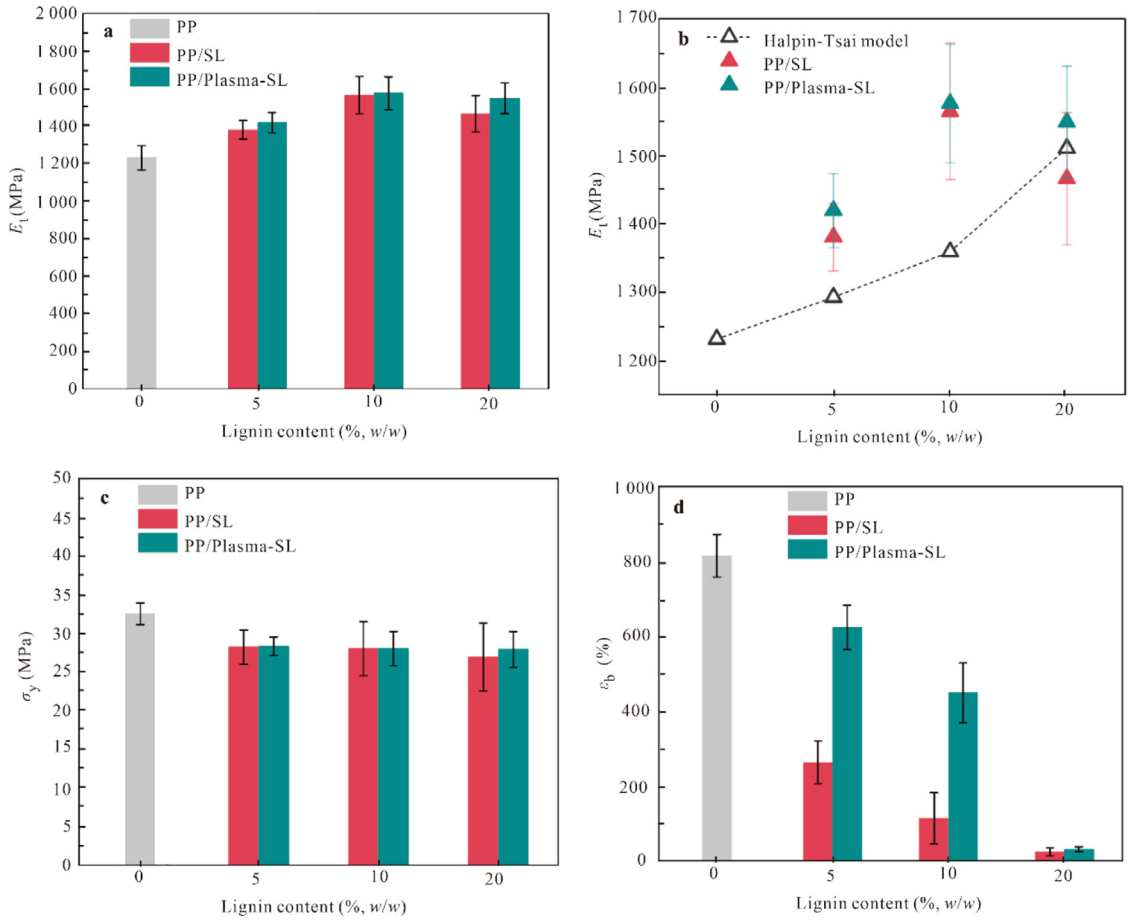
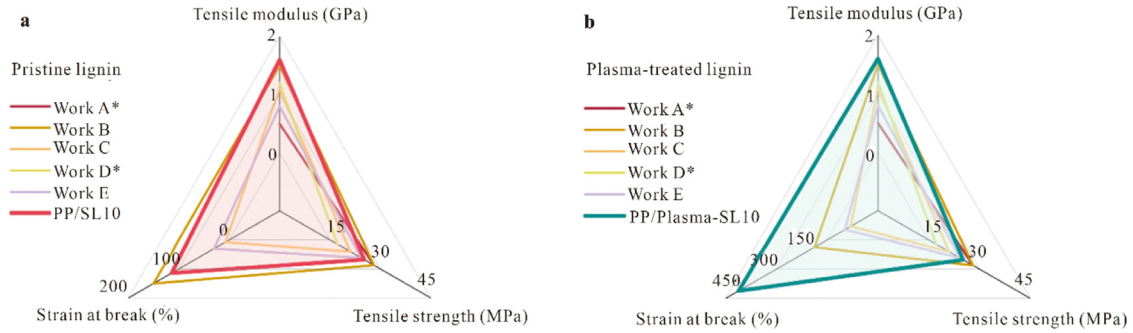



**Fig. 7.** Results of tensile tests of PP and PP/lignin blends. (a) Tensile modulus ($E_t$); (b) Comparison between experimental and predicted values according to the Halpin-Tsai model for PP/lignin blends tensile modulus ($E_t$); (c) Yield strength ($\sigma_y$); (d) Strain at break ($\varepsilon_b$).

more homogeneous results with reduced variability (i.e., lower statistical deviation) in the measured $\sigma_y$ values, likely stemming from the improved dispersion achieved for treated lignin.

From the perspective of mechanical performance, one of the main drawbacks often encountered in PP/lignin blends was their limited ability to attain high strains. Indeed, lignin particles were known to easily promote crack initiation and propagation during elongation as a result of their poor miscibility with PP (Wang et al., 2024). Interestingly, in the present study, a strikingly positive impact of lignin plasma treatment on the ultimate elongation properties of PP/lignin blends was observed. As shown in Fig. 7d, the $\varepsilon_b$ values for PP/Plasma-SL blends were consistently higher than PP/SL systems for all the lignin contents investigated. On average, Plasma-SL provided an increase in strain at break of about 137%, 294%, and 30% for blends containing 5%, 10%, and 20% (*w/w*) of lignin, respectively, compared to blends containing the same amount of pristine SL. This positive result could be attributed to the improved compatibility between the lignin filler and the PP matrix achieved through plasma treatment. In particular, the significant reduction in the concentration of lignin hydroxyl and carboxyl species (~30%) resulting from the plasma process (Section 3.1 and Section 3.2) led to enhanced lignin-PP affinity and promoted a stronger interfacial interaction, which was accountable for the improved mechanical performance. Furthermore, plasma treatment introduced new active sites on the lignin structure (i.e., phenoxy radicals), which were likely to enable the formation of grafted species (Coiai et al., 2017), further contributing to reinforcing the matrix-filler interface. As a result, blends containing 5% (*w/w*) and 10% (*w/w*) lignin could achieve $\varepsilon_b$ values of up to 680% and 530%, respectively. At higher lignin content (20%, *w/w*), the elongation at break decreased significantly due to insufficient filler-matrix adhesion (Figs. S4 and S5), leading to a transition from a ductile to a more brittle behavior. This observation was in line with the results from the rheological tests discussed above and confirmed the detrimental effect of high lignin content on the mechanical properties of the blend.

It was worth highlighting that the elongation values achieved in this work were largely above those typically obtained in chemically modified PP/lignin blends (e.g., by lignin alkylation) and by making use of compatibilizers (e.g., MAn-g-PP) (Chen et al., 2011; Dias et al., 2019; Karina et al., 2017; Tian et al., 2022). Most importantly, the present plasma-based process guaranteed maximum elongation values that were higher than those achieved using other non-chemical lignin treatments on average




*, strain at break data were not available.

**Fig. 8.** Comparison of mechanical properties of (a) PP/SL10 and (b) PP/Plasma-SL10 and PP/lignin blends containing 10% (*w/w*) lignin with different lignin compatibilization strategies (Sources: A, Chen et al., 2011; B, Iyer and Torkelson, 2015; C, Karina et al., 2017; D, Dias et al., 2019; E, Jalaee et al., 2024.).

**Table 4**
Property retention rate for tensile modulus ($R_{E_t}$), yield strength ($R_{\sigma_y}$), yield strain ($R_{\varepsilon_y}$), strain at break ($R_{\varepsilon_b}$) after one additional extrusion step for neat PP, PP/SL5, and PP/Plasma-SL5.

| Sample Name | $R_{E_t}$ (%) | $R_{\sigma_y}$ (%) | $R_{\varepsilon_y}$ (%) | $R_{\varepsilon_b}$ (%) |
|---|---|---|---|---|
| PP | 87.0 ± 1.2 | 96.0 ± 3.7 | 89.5 ± 0.9 | 94.6 ± 3.5 |
| PP/SL5 | 92.0 ± 0.7 | 96.5 ± 5.4 | 96.1 ± 2.0 | 95.4 ± 7.1 |
| PP/Plasma-SL5 | 92.0 ± 0.1 | 98.2 ± 2.4 | 97.5 ± 0.1 | 98.4 ± 2.2 |

(i.e., size reduction), while concurrently preserving optimal tensile strength and attaining high tensile modulus values (Iyer and Torkelson, 2015; Jalaee et al., 2024), further validating the GAT plasma treatment as chemical-free compatibilization method. This was also reflected in the significantly higher fracture energy values obtained in blends incorporating plasma-treated lignin and untreated one (see Table S3). For comparative purposes, the data discussed above were illustrated in the charts of Fig. 8, in which the mechanical performance, including tensile modulus, tensile strength (here corresponding to yield strength), and strain at break of PP blends containing 10% (*w/w*) SL and Plasma-SL (i.e., PP/SL10 and PP/Plasma-SL10, respectively) was presented in comparison to literature values for PP/lignin blends of corresponding lignin-content (additional data were available in Table S4).

To assess the impact of reprocessing on the mechanical properties of neat PP and PP/lignin blends, tensile tests were also carried out on PP, PP/SL5 (PP with 5% (*w/w*) SL) and PP/Plasma-SL5 (PP with 5% (*w/w*) Plasma-SL) after a second twin-screw extrusion step, and the mechanical response of the obtained reprocessed blends was compared with the corresponding as-prepared materials (Fig. 9). In addition, the material-property retention rate for each system was evaluated according to Eq. (7) (Table 4). As mentioned before, thermo-mechanical reprocessing of PP generally caused its partial degradation, leading to the formation of lower molecular weight fractions by chain scission with a consequent negative effect on the mechanical performance of the material (Grassie, 1983; Saikrishnan et al., 2020).

As expected, after the second extrusion step, all the materials experienced a slight reduction in mechanical response (Fig. 9). However, it was noteworthy that the presence of lignin in the blends appeared to partly mitigate such deterioration of mechanical properties, as evidenced by the higher retention rates in PP/lignin blends and PP reported in Table 4. This effect might be attributed to the well-demonstrated antioxidant ability of lignin, which inhibited the activity of free radicals, thereby preserving the macromolecular structure and properties of the virgin PP matrix (Pouteau et al., 2003; Cicala et al., 2017; Chen and Zhang, 2019). Remarkably, in the presence of plasma-treated lignin, such beneficial effects on the mechanical properties of the PP/lignin blend appeared even more pronounced. This result was in line with the outcomes of TGA and dynamic frequency sweep measurements, in which the improved compatibility of plasma-treated lignin with PP was discussed concerning its increased antioxidant activity. In this context, the use of plasma-treated lignin as an additive in PP/lignin compounds might also represent a viable strategy to boost their thermo-mechanical reprocessability without significantly affecting their mechanical response.

## 4. Conclusions

In this study, a new lignin compatibilization physical method for the production of high-performance PP/lignin blends was presented. Soda lignin was subjected to plasma treatment in an argon atmosphere employing a GAT configuration, ensuring an optimal mixing of lignin powder with the carrier gas, leading to improved treatment. EPR and $^{31}$P NMR measurements on plasma-treated

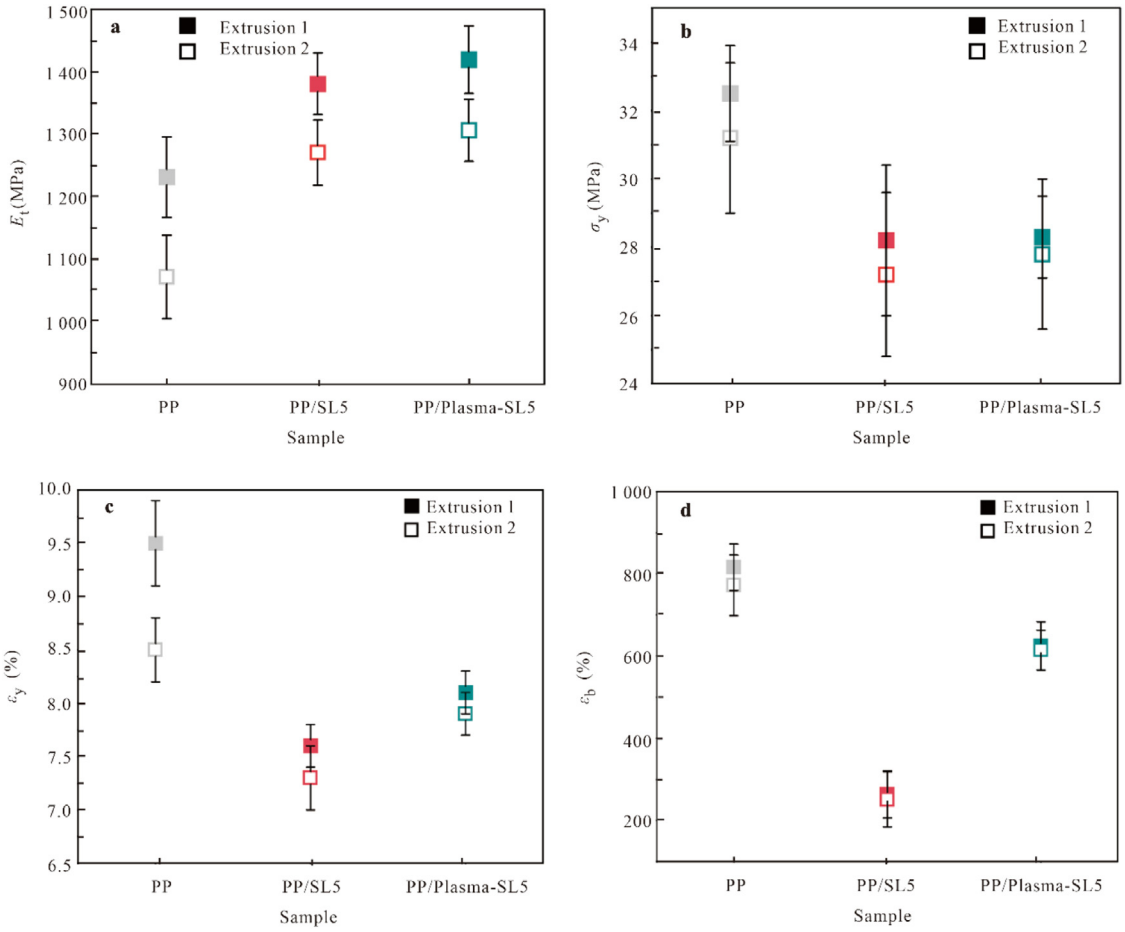



**Fig. 9.** Tensile properties after the second extrusion and properties obtained before reprocessing. (a) Tensile modulus ($E_t$); (b) Yield strength ($\sigma_y$); (c) Yield strain ($\varepsilon_y$); (d) Strain at break ($\varepsilon_b$).

lignin showed an increased concentration of phenoxy radicals of >60%, and a concurrent reduction in aliphatic and phenolic hydroxyl functionalities of about 39% and 30%, respectively, for pristine lignin. Moreover, DSC and TGA revealed the formation of a more condensed lignin structure as a result of the plasma process, characterized by an increased $T_g$ and enhanced thermo-oxidative stability. In particular, the incorporation of 5% (*w*/*w*), 10% (*w*/*w*), and 20% (*w*/*w*) of lignin (both pristine and plasma-treated) was found to promote the formation of a homogeneous $\alpha$-crystalline phase in the PP matrix, without affecting the PP melting temperature (~165 ˚C). As a result of the radical scavenging ability of lignin, a remarkable increase in the thermo-oxidative stability of the PP/lignin material could be observed for progressively higher lignin contents. Due to its highly condensed structure and lower concentration of polar (–OH, –COOH) functionalities, such antioxidant effect was shown to be more pronounced in blends incorporating plasma-treated lignin. This result was supported by dynamic rheological frequency sweep analysis, which showed longer relaxation times for PP/Plasma-SL blends, as a result of the preservation of the average macromolecular chain length in these blends (i.e., no degradative chain-scission phenomena). In addition, the higher shear viscosity measured in PP/Plasma-SL blends further evidenced the enhanced interaction between Plasma-SL particles and PP. Mechanical testing revealed that Young's modulus of the PP/lignin blends increased markedly upon lignin addition, reaching up to 1 576 MPa in PP/Plasma-SL10 compared to 1 200 MPa for neat PP. This trend was accompanied by a slight reduction of yield strength, which was found to be ~28 MPa in PP/lignin blends and 32 MPa for neat PP. Remarkably, PP/Plasma-SL systems exhibited substantially higher strain at break than the corresponding blends based on pristine lignin, both at 5% (*w*/*w*) (~260% in PP/SL5, ~625% in PP/Plasma-SL5) and at 10% (*w*/*w*) (~115% in PP/SL10, ~450% in PP/Plasma-SL10) lignin content. Furthermore, following the second twin-screw extrusion process as representative of a thermo-mechanical reprocessing cycle, the PP/lignin blends containing Plasma-SL showed slightly better retention of mechanical performances compared to both pure PP and PP blends incorporating pristine lignin, particularly considering the nearly unmodified (retention rate ≈ 95%) strain at break. This work demonstrates the effectiveness of plasma treatment as a viable and eco-friendly strategy to improve PP-lignin compatibility without the use of solvents, molecular compatibilizers or additional chemical steps, paving the way for the development of high bio-carbon-content thermoplastic materials incorporating lignin with enhanced thermo-mechanical characteristics and improved reprocessability.

## Declaration of competing interest

The authors declare that they have no known competing financial interests or personal relationships that could have appeared to influence the work reported in this paper.

## Acknowledgements

This work received funding from Regione Lombardia and Fondazione Cariplo (No. 2018-1739, Project: POLISTE), the European Union's Horizon 2020 Research and Innovation Programme (No. 952941, Project: BIOMAC), and Regione Lombardia ("Collaboration Agreement for the Creation of an Innovative Pilot Regional Infrastructure to Support the Transition Towards the Circular Economy", Project: EcoCIRC Regional Hub). This study was partly carried out within the Agritech National Research Center funded by the European Union Next-GenerationEU (National Recovery and Resilience Plan (Piano Nazionale di Ripresa e Resilienza - PNRR) – Mission 4, Component 2, Investment line 1.4 – d.d. 1032 17/06/2022, cn00000022). Part of the research was performed also within the MUSA – Multilayered Urban Sustainability Action – project, funded by the European Union Next-GenerationEU (National Recovery and Resilience Plan (Piano Nazionale di Ripresa e Resilienza - PNRR) – Mission 4, Component 2, Investment line 1.5: Strengthening of Research Structures and Creation of R&D "Innovation Ecosystems", Set Up of "Territorial Leaders in R&D).

## Supplementary materials

Supplementary material associated with this article can be found, in the online version, at doi:10.1016/j.jobab.2025.01.003.

## References

Abdelwahab, M.A., Misra, M., Mohanty, A.K., 2019. Injection molded biocomposites from polypropylene and lignin: effect of compatibilizers on interfacial adhesion and performance. Ind. Crops Prod. 132, 497–510.
Alexy, P., Košíková, B., Crkonová, G., Gregorová, A., Martiš, P., 2004. Modification of lignin-polyethylene blends with high lignin content using ethylene-vinylacetate copolymer as modifier. J. Appl. Polym. Sci. 94, 1855–1860.
Anushikha, Gaikwad, K.K., 2023. Lignin as a UV blocking, antioxidant, and antimicrobial agent for food packaging applications. Biomass Convers. Biorefin. 14, 16755–16767.
Atifi, S., Miao, C.W., Hamad, W.Y., 2017. Surface modification of lignin for applications in polypropylene blends. J. Appl. Polym. Sci. 134, e45103.
Atz Dick, T., Couve, J., Gimello, O., Mas, A., Robin, J.J., 2017. Chemical modification and plasma-induced grafting of pyrolitic lignin. Evaluation of the reinforcing effect on lignin/poly(L-lactide) composites. Polymer (Guildf) 118, 280–296.
Balakshin, M., Capanema, E., 2015. On the quantification of lignin hydroxyl groups with $^{31}$P and $^{13}$C NMR spectroscopy. J. Wood Chem. Technol. 35, 220–237.
Barnes, H.A., 2000. A Handbook of Elementary Rheology. University of Wales, Institute of Non-Newtonian Fluid Mechanics.
Barni, R., Alex, P., Salanti, A., Canevali, C., Zoia, L., Orlandi, M., Riccardi, C., 2021. Characterization of the electrical and optical properties of a gliding arc tornado device. Eur. Phys. J. D 75, 147.
Barni, R., Canevali, C., Zoia, L., Orlandi, M., Bellinetto, E., Boumezgane, O., Turri, S., Griffini, G., Riccardi, C., 2022. Plasma processing of nano and microparticles in gliding arc tornado device. The 48th EPS Conference Plasma Physics, EPS 2022.
Barni, R., Canevali, C., Zoia, L., Orlandi, M., Bellinetto, E., Boumezgane, O., Turri, S., Griffini, G., Riccardi, C., 2023. Characterization of a gliding arc tornado device for lignin particles functionalization. The 49th EPS Conference Plasma Physics, EPS 2023.
Beckert, D., Burkitt, M., Canters, G., Groenen, E., Collison, D., McInnes, E., Eaton, G.R., Eaton, S.S., Giamello, E., Huttermann, J., Kappl, R., Kay, C., Weber, S., Lurie, D., Smirnov, A., Smith, G., Riedi, P., 2002. Electron Paramagnetic Resonance In: Gilbert, B.C., Davies, M.J., Murphy, D.M. (Eds.). Royal Society of Chemistry, London.
Bellinetto, E., Fumagalli, N., Astorri, M., Turri, S., Griffini, G., 2024. Elucidating the role of lignin type and functionality in the development of high-performance biobased phenolic thermoset resins. ACS Appl. Polym. Mater. 6, 1191–1203.
Bertella, S., Luterbacher, J.S., 2020. Lignin functionalization for the production of novel materials. Trends. Chem. 2, 440–453.
Canetti, M., Bertini, F., De Chirico, A., Audisio, G., 2006. Thermal degradation behaviour of isotactic polypropylene blended with lignin. Polym. Degrad. Stab. 91, 494–498.
Cao, Y.Z., Tang, M., Yang, P., Chen, M.Z., Wang, S.Q., Hua, H.M., Chen, W.M., Zhou, X.Y., 2020. Atmospheric low-temperature plasma-induced changes in the structure of the lignin macromolecule: an experimental and theoretical investigation. J. Agric. Food Chem. 68, 451–460.
Carri, G.A., Winter, H.H., 1997. Mapping of the relaxation patterns of polymer melts with linear flexible molecules of uniform length. Rheol. Acta 36, 330–344.
Chen, F., Dai, H.H., Dong, X.L., Yang, J.T., Zhong, M.Q., 2011. Physical properties of lignin-based polypropylene blends. Polym. Compos. 32, 1019–1025.
Chen, F.G., Zhang, M.Z., 2019. Maleic anhydride-modified polyolefins as compatibilizer for lignin-reinforced polypropylene composites. Polym. Compos. 40, 2594–2601.
Cicala, G., Tosto, C., Latteri, A., La Rosa, A.D., Blanco, I., Elsabbagh, A., Russo, P., Ziegmann, G., 2017. Green composites based on blends of polypropylene with liquid wood reinforced with hemp fibers: thermomechanical properties and the effect of recycling cycles. Materials (Basel) 10, 998.
Coiai, S., Cicogna, F., Yang, C.C., Tempesti, V., Carroccio, S.C., Gorrasi, G., Mendichi, R., Dintcheva, N.T., Passaglia, E., 2017. Grafting of hindered phenol groups onto ethylene/$\alpha$-olefin copolymer by nitroxide radical coupling. Polymers (Basel) 9, 670.
Constant, S., Wienk, H.L.J., Frissen, A.E., de Peinder, P., Boelens, R., van Es, D.S., Grisel, R.J.H., Weckhuysen, B.M., Huijgen, W.J.J., Gosselink, R.J.A., Bruijnincx, P.C.A., 2016. New insights into the structure and composition of technical lignins: a comparative characterisation study. Green Chem. 18, 2651–2665.
Dias, O.A.T., Sain, M., Cesarino, I., Leão, A.L., 2019. Development of high bio-content polypropylene composites with different industrial lignins. Polym. Adv. Technol. 30, 70–78.
Domínguez, J.C., Oliet, M., Alonso, M.V., Gilarranz, M.A., Rodríguez, F., 2008. Thermal stability and pyrolysis kinetics of organosolv lignins obtained from *Eucalyptus globulus*. Ind. Crops Prod. 27, 150–156.
Duval, A., Lawoko, M., 2014. A review on lignin-based polymeric, micro- and nano-structured materials. React. Funct. Polym. 85, 78–96.
Elmoumni, A., Winter, H.H., Waddon, A.J., Fruitwala, H., 2003. Correlation of material and processing time scales with structure development in isotactic polypropylene crystallization. Macromolecules 36, 6453–6461.
Gadioli, R., Waldman, W.R., de Paoli, M.A., 2016. Lignin as a green primary antioxidant for polypropylene. J. Appl. Polym. Sci. 133, e43558.
Geyer, R., Jambeck, J.R., Law, K.L., 2017. Production, use, and fate of all plastics ever made. Sci. Adv. 3, e1700782.
Grassie, N., 1983. Degradation and stabilisation of polyolefins. In: Allen, N.S (Ed.), Polymer Degradation and Stability. Elsevier Applied Science Publishers, London.
Gregorová, A., Cibulková, Z., Košíková, B., Šimon, P., 2005. Stabilization effect of lignin in polypropylene and recycled polypropylene. Polym. Degrad. Stab. 89, 553–558.
Guilhen, A., Gadioli, R., Fernandes, F.C., Waldman, W.R., Aurelio De Paoli, M., 2017. High-density green polyethylene biocomposite reinforced with cellulose fibers and using lignin as antioxidant. J. Appl. Polym. Sci. 134, e45219.

Halpin, J.C., 1969. Stiffness and expansion estimates for oriented short fiber composites. J. Compos. Mater. 3, 732–734.
Hon, D.N.S., 1992. Electron spin resonance (ESR) spectroscopy. In: Lin, S.Y., Dence, C.W. (Eds.), Springer Series in Wood Science. Springer, Heidelberg, pp. 274–286.
Iyer, K.A., Torkelson, J.M., 2015. Sustainable green hybrids of polyolefins and lignin yield major improvements in mechanical properties when prepared via solid-state shear pulverization. ACS Sustainable Chem. Eng. 3, 959–968.
Jalaee, A., Trottman, K., French, V., Raghunath, S., Brito dos Santos, F., Foster, E.J., 2024. Improved thermomechanical and rheological properties of polypropylene composites with thermomechanical pulp for injection molding. Polym. Compos. 45, 12782–12795.
Kabir, A.S., Yuan, Z.S., Kuboki, T., Xu, C.B., 2019. Development of lignin-based antioxidants for polymers. In: Fang, Z., Smith, R.L., Tian, X.F. (Eds.), Production of Materials from Sustainable Biomass Resources. Springer, Singapore, pp. 39–59.
Kalra, C.S., Cho, Y.I., Gutsol, A., Fridman, A., Rufael, T.S., 2005. Gliding arc in tornado using a reverse vortex flow. Rev. Sci. Instrum. 76, 025110.
Karina, M., Syampurwadi, A., Satoto, R., Irmawati, Y., Puspitasari, T., 2017. Physical and mechanical properties of recycled polypropylene composites reinforced with rice straw lignin. Bioresources 12, 5801–5811.
Klarhöfer, L., Viöl, W., Maus-Friedrichs, W., 2010. Electron spectroscopy on plasma treated lignin and cellulose. Holzforschung 64, 331–336.
Kun, D., Pukánszky, B., 2017. Polymer/lignin blends: interactions, properties, applications. Eur. Polym. J. 93, 618–641.
Lee, J.H., Jang, D., Yang, I., Jo, S.M., Lee, S., 2022. Effect of phosphorylated lignin on flame retardancy of polypropylene-based composites. J. Appl. Polym. Sci. 139, e52519.
Lee, K.T., Goddard, J.M., Hotchkiss, J.H., 2009. Plasma modification of polyolefin surfaces. Packag. Technol. Sci. 22, 139–150.
Levchenko, I., Mandhakini, M., Prasad, K., Bazaka, O., Ivanova, E.P., Jacob, M.V., Baranov, O., Riccardi, C., Roman, H.E., Xu, S.Y., Bazaka, K., 2022. Functional nanomaterials from waste and low-value natural products: a technological approach level. Adv. Mater. Technol. 7, 2101471.
Li, Y.M., Cui, D.X., Tong, Y.J., Xu, L.H., 2013. Study on structure and thermal stability properties of lignin during thermostabilization and carbonization. Int. J. Biol. Macromol. 62, 663–669.
Lima, M.F.S., Vasconcellos, M.A.Z., Samios, D., 2002. Crystallinity changes in plastically deformed isotactic polypropylene evaluated by X-ray diffraction and differential scanning calorimetry methods. J. Polym. Sci. Part B Polym. Phys. 40, 896–903.
Liston, E.M., Martinu, L., Wertheimer, M.R., 1993. Plasma surface modification of polymers for improved adhesion: a critical review. J. Adhes. Sci. Technol. 7, 1091–1127.
Lobato-Peralta, D.R., Duque-Brito, E., Villafán-Vidales, H.I., Longoria, A., Sebastian, P.J., Cuentas-Gallegos, A.K., Arancibia-Bulnes, C.A., Okoye, P.U., 2021. A review on trends in lignin extraction and valorization of lignocellulosic biomass for energy applications. J. Clean. Prod. 293, 126123.
Lotz, B., 1998. $\alpha$ and $\beta$ phases of isotactic polypropylene: a case of growth kinetics 'phase reentrency' in polymer crystallization. Polymer (Guildf) 39, 4561–4567.
Lu, F.F., Yu, H.Y., Yan, C.F., Yao, J.M., 2016. Polylactic acid nanocomposite films with spherical nanocelluloses as efficient nucleation agents: effects on crystallization, mechanical and thermal properties. RSC Adv. 6, 46008–46018.
Luo, S.P., Cao, J.Z., McDonald, A.G., 2017. Esterification of industrial lignin and its effect on the resulting poly(3-hydroxybutyrate-co-3-hydroxyvalerate) or polypropylene blends. Ind. Crops Prod. 97, 281–291.
Maldhure, A.V., Chaudhari, A.R., Ekhe, J.D., 2010. Thermal and structural studies of polypropylene blended with esterified industrial waste lignin. J. Therm. Anal. Calorim. 103, 625–632.
Miao, C.W., Hamad, W.Y., 2017. Controlling lignin particle size for polymer blend applications. J. Appl. Polym. Sci. 134, e44669.
Moan, M., Huitric, J., Médéric, P., Jarrin, J., 2000. Rheological properties and reactive compatibilization of immiscible polymer blends. J. Rheol. 44, 1227–1245.
Moliton, J.P., Jussiaux, C., Trigaud, T., Lazzaroni, R., Lhost, O., Bredas, J.L., Kihn, Y., Sevely, J., 1996. Relation between plasmons and the valence-band density of states in polymethylmethacrylate: influence of ion irradiation on damage selectivity. Philos. Mag. B 73, 763–778.
Müller, K., Zollfrank, C., Schmid, M., 2019. Natural polymers from biomass resources as feedstocks for thermoplastic materials. Macromol. Mater. Eng. 304, 1–17.
Novais, R.M., Simon, F., Paiva, M.C., Covas, J.A., 2012. The influence of carbon nanotube functionalization route on the efficiency of dispersion in polypropylene by twin-screw extrusion. Compos. Part A Appl. Sci. Manuf. 43, 2189–2198.
Patil, S.V., Argyropoulos, D.S., 2017. Stable organic radicals in lignin: a review. ChemSusChem 10, 3284–3303.
Patrício Silva, A.L., Prata, J.C., Walker, T.R., Campos, D., Duarte, A.C., Soares, A.M.V.M., Barcelò, D., Rocha-Santos, T., 2020. Rethinking and optimising plastic waste management under COVID-19 pandemic: policy solutions based on redesign and reduction of single-use plastics and personal protective equipment. Sci. Total Environ. 742, 140565.
Pouteau, C., Baumberger, S., Cathala, B., Dole, P., 2004. Lignin-polymer blends: evaluation of compatibility by image analysis. C. R. Biol. 327, 935–943.
Pouteau, C., Dole, P., Cathala, B., Averous, L., Boquillon, N., 2003. Antioxidant properties of lignin in polypropylene. Polym. Degrad. Stab. 81, 9–18.
Rabinovich, A., Nirenberg, G., Kocagoz, S., Surace, M., Sales, C., Fridman, A., 2022. Scaling up of non-thermal gliding arc plasma systems for industrial applications. Plasma Chem. Plasma Process. 42, 35–50.
Ridho, M.R., Agustiany, E.A., Rahmi Dn, M., Madyaratri, E.W., Ghozali, M., Restu, W.K., Falah, F., Rahandi Lubis, M.A., Syamani, F.A., Nurhamiyah, Y., Hidayati, S., Sohail, A., Karungamye, P., Nawawi, D.S., Iswanto, A.H., Othman, N., Mohamad Aini, N.A., Hussin, M.H., Sahakaro, K., Hayeemasae, N., Ali, M.Q., Fatriasari, W., 2022. Lignin as green filler in polymer composites: development methods, characteristics, and potential applications. Adv. Mater. Sci. Eng. 2022, 1363481.
Sadeghifar, H., Ragauskas, A., 2020. Lignin as a UV light blocker-a review. Polymers (Basel) 12, 1134.
Saikrishnan, S., Jubinville, D., Tzoganakis, C., Mekonnen, T.H., 2020. Thermo-mechanical degradation of polypropylene (PP) and low-density polyethylene (LDPE) blends exposed to simulated recycling. Polym. Degrad. Stab. 182, 109390.
Saito, T., Brown, R.H., Hunt, M.A., Pickel, D.L., Pickel, J.M., Messman, J.M., Baker, F.S., Keller, M., Naskar, A.K., 2012. Turning renewable resources into value-added polymer: development of lignin-based thermoplastic. Green Chem. 14, 3295–3303.
Sakai, H., Kuroda, K., Muroyama, S., Tsukegi, T., Kakuchi, R., Takada, K., Hata, A., Kojima, R., Ogoshi, T., Omichi, M., Ninomiya, K., Takahashi, K., 2018. Alkylated alkali lignin for compatibilizing agents of carbon fiber-reinforced plastics with polypropylene. Polym. J. 50, 281–284.
Scarica, C., Suriano, R., Levi, M., Turri, S., Griffini, G., 2018. Lignin functionalized with succinic anhydride as building block for biobased thermosetting polyester coatings. ACS Sustainable Chem. Eng. 6, 3392–3401.
Souza, J.R., Araujo, J.R., Archanjo, B.S., Simão, R.A., 2019. Cross-linked lignin coatings produced by UV light and $SF_6$ plasma treatments. Prog. Org. Coat. 128, 82–89.
Stanzione III, J., La Scala, J., 2016. Sustainable polymers and polymer science: dedicated to the life and work of Richard P. Wool. J. Appl. Polym. Sci. 133, e44212.
Tanks, J., Tamura, K., Naito, K., Nge, T.T., Yamada, T., 2023. Glycol lignin/MAH-g-PP blends and composites with exceptional mechanical properties for automotive applications. Compos. Sci. Technol. 238, 110030.
Tian, B., Li, J.F., Li, Z.G., Dong, W., Zhang, N., Zhao, H.T., Liu, Y.G., Di, M.W., 2022. Preparation of polypropylene with high melt strength by wet reaction blending of lignin. J. Appl. Polym. Sci. 139, e51224.
Toriz, G., Denes, F., Young, R.A., 2002. Lignin-polypropylene composites. Part 1: composites from unmodified lignin and polypropylene. Polym. Compos. 23, 806–813.
Vega, J.F., Rastogi, S., Peters, G.W.M., Meijer, H.E.H., 2004. Rheology and reptation of linear polymers. Ultrahigh molecular weight chain dynamics in the melt. J. Rheol. 48, 663–678.
Wang, R.C., You, X.Y., Qi, S.J., Tian, R.Y., Zhang, H.J., 2024. Enhancing mechanical performance of high-lignin-filled polypropylene via reactive extrusion. Polymers (Basel) 16, 520.
Wang, S.X., Muiruri, J.K., Soo, X.Y.D., Liu, S.L., Thitsartarn, W., Tan, B.H., Suwardi, A., Li, Z.B., Zhu, Q., Loh, X.J., 2023. Bio-polypropylene and polypropylene-based biocomposites: solutions for a sustainable future. Chem. Asian J. 18, e202200972.
Weil, J.A., Bolton, J.R., 2006. Electron Paramagnetic Resonance: Elementary Theory and Practical Applications. John Wiley & Sons, Hoboken.
Ye, D.Z., Li, S., Lu, X.M., Zhang, X., Rojas, O.J., 2016. Antioxidant and thermal stabilization of polypropylene by addition of butylated lignin at low loadings. ACS Sustainable Chem. Eng. 4, 5248–5257.
Yeo, J.S., Seong, D.W., Hwang, S.H., 2015. Chemical surface modification of lignin particle and its application as filler in the polypropylene composites. J. Ind. Eng. Chem. 31, 80–85.
Zaitsev, A., Moisan, S., Poncin-Epaillard, F., 2018. Study of the alkali lignin stabilization thanks to plasma process. Polym. Degrad. Stab. 156, 202–210.

Zanini, S., Canevali, C., Orlandi, M., Tolppa, E.L., Zoia, L., Riccardi, C., Morazzoni, F., 2008. Radical formation on CTMP fibers by argon plasma treatments and related lignin chemical changes. Bioresources 3, 995–1009.
Zanini, S., Riccardi, C., Canevali, C., Orlandi, M., Zoia, L., Tolppa, E.L., 2005. Modifications of lignocellulosic fibers by Ar plasma treatments in comparison with biological treatments. Surf. Coat. Technol. 200, 556–560.
Zare, Y., 2016. Development of Halpin-Tsai model for polymer nanocomposites assuming interphase properties and nanofiller size. Polym. Test. 51, 69–73.
Zhao, X.J., Liu, Y.H., Sun, B.H., Liu, Z.C., Shao, Z.B., Liu, X.B., Zhang, H.L., Sun, Z.Y., Hu, W., 2023. Lignin-derived flame retardant for improving fire safety and mechanical properties of polypropylene. J. Appl. Polym. Sci. 140, e54739.